International Journal of Pharmaceutics 682 (2025) 125952

Contents lists available at ScienceDirect

International Journal of Pharmaceutics

journal homepage: www.elsevier.com/locate/ijpharm

Development of inhalable spray dried nalbuphine hydrochloride powders

Waiting Tai [a], Hong-Jaan Wang [b], Dipesh Khanal [a], Pancy Tsz Hei Kwong [a], Patricia Tang [a], Chih-Chin Shih [c,*], Hak-Kim Chan [a,*]

[a] Advanced Drug Delivery Group, Sydney Pharmacy School, Faculty of Medicine and Health, The University of Sydney, Sydney, NSW 2006, Australia
[b] School of Pharmacy, National Defense Medical Center, Taipei, Taiwan, Republic of China
[c] Department and Graduate Institute of Pharmacology, National Defense Medical Center, Taipei, Taiwan, Republic of China

ARTICLE INFO

Keywords:
Nalbuphine hydrochloride
Opioids
Inhalation
Pulmonary delivery
Dry powder formulation
Leucine
Human serum albumin

ABSTRACT

Nalbuphine hydrochloride (NAL) is a potent opioid analgesic that has been used clinically for decades. However, current delivery methods are either invasive or inefficient due to low bioavailability. Therefore, an alternative route of administration is needed. Pulmonary delivery is a promising option as it can provide high bioavailability and a rapid onset of action. Beyond systemic analgesia, NAL has also shown local therapeutic benefits in the lungs. This study aimed to develop inhalable NAL powders using spray drying, with leucine and human serum albumin (HSA) as dispersion enhancers. The resulting powders were amorphous and contained <4 % residual solvent by mass. The spray dried particles were spherical, 3–4 μm large, and exhibited corrugated surface. Spray dried NAL alone were inhalable, with a fine particle fraction <5 μm (FPF) at 25 %. The addition of HSA improved the FPF to 33 % and 37 % for 10 % and 20 % w/w HSA, respectively. Similarly, the FPF increased to 39 % after adding 10 % w/w leucine, reaching a maximum of 47 % with 20 % w/w leucine. The latter formulation also demonstrated good chemical and physical stability after one month of storage at 25 °C under both 30 % and 60 % relative humidity. These formulations can be used as a platform to deliver NAL and other opioid analgesics by inhalation.

1. Introduction

Nalbuphine hydrochloride (NAL) has been used clinically for decades as a potent analgesic. It is a semi-synthetic opioid that is equipotent to morphine (Liang et al., 2020). However, unlike morphine, which is a full mu opioid receptor agonist, NAL acts as a mu opioid receptor antagonist and a kappa opioid receptor agonist (Chen et al., 2024). These mechanistic differences confer NAL a more favourable safety profile, with fewer adverse effects and a lower risk of addiction. Due to its low abuse potential, NAL is the only opioid in the United States that is not classified as a controlled substance (Narver, 2015).

NAL is primarily administered as a solution for intravenous, intramuscular, and subcutaneous injection. Although oral NAL tablets are available, their use is limited due to low oral bioavailability (11–25 %) (Tymko et al., 2024; Wang et al., 2014). To improve its delivery, previous studies have explored alternative route of administration, including rectal and intranasal delivery. While rectal NAL was rapidly absorbed and provided adequate analgesia, it exhibited high inter-individual pharmacokinetic (PK) variability, likely due to the inclusion of paediatric subjects, who naturally have more variable PK profiles than adults (Kuznetsov and Tymko, 2024). In contrast, intranasal administration demonstrated a bioavailability of 65 % (Tymko et al., 2024) and has proven effective in treating pain associated with conditions such as prehospital trauma (Pietsch et al., 2021) and post-operative recovery (Tymko et al., 2024), supporting its clinical feasibility. Based on this, a pharmaceutical company in Ukraine developed a NAL nasal spray, Apain® (Tymko et al., 2024; Tymko et al., 2023). Although its official dosing instructions are unavailable, human PK and efficacy studies used a 10.5 mg dose (administered as three sprays) at intervals of every 5–6 h, consistent with the 5-h plasma half-life of NAL (Tymko et al., 2024; Tymko et al., 2023). However, frequent intranasal administration may damage the nasal mucosa. Moreover, concentrated aqueous NAL solutions (i.e. 25 mg/mL in water) are chemically unstable due to oxidative degradation and precipitation at low temperatures (Kuznetsov and Tymko, 2023). For instance, Apain solutions reportedly changed colour from light blue to pink after prolonged storage, although they remained stable at room temperature for at least 28 days (Kuznetsov and Tymko, 2024). Such instability raises concerns about

* Corresponding authors.
E-mail addresses: ccshih@mail.ndmctsgh.edu.tw (C.-C. Shih), kim.chan@sydney.edu.au (H.-K. Chan).

https://doi.org/10.1016/j.ijpharm.2025.125952
Received 15 May 2025; Received in revised form 4 July 2025; Accepted 7 July 2025
Available online 9 July 2025

Table 1
Solute mass ratios of the spray dried formulations.

Formulations	Nalbuphine	Leucine	Human serum albumin (HSA)
SD NAL	100 %	0 %	0 %
NAL10L	90 %	10 %	0 %
NAL10HSA	90 %	0 %	10 %
NAL20L	80 %	20 %	0 %
NAL20HSA	80 %	0 %	20 %

Table 2
The production yields, volumetric diameters, and spans of the spray dried formulations.

Formulations	Production yield (%)	D_{10} (μm)	D_{50} (μm)	D_{90} (μm)	Span
SD NAL	80.4	0.7 ± 0.1	2.8 ± 0.1	6.3 ± 0.3	2.0 ± 0.1
NAL10L	84.5	0.6 ± 0.1	3.2 ± 0.1	7.7 ± 0.9	2.3 ± 0.2
NAL10HSA	83.9	0.9 ± 0.1	3.5 ± 0.1	7.1 ± 0.8	1.8 ± 0.2
NAL20L	84.6	0.7 ± 0.1	3.7 ± 0.2	6.8 ± 0.3	1.6 ± 0.1
NAL20HSA	79.2	1.1 ± 0.1	3.9 ± 0.1	7.7 ± 0.2	1.7 ± 0.1

efficacy loss, exposure to degradation products, and safety risks.

To address these issues, a promising alternative is pulmonary delivery of NAL in the form of inhalable powders. Pulmonary delivery has been shown to achieve high bioavailability, rapid onset of action, less adverse effects, and improved convenience and tolerance across various populations (Tai and Kwok, 2022). These advantages have already been demonstrated with inhaled opioids such as fentanyl, which achieved comparable bioavailability and time to reach maximum concentration than intravenous injection (Macleod et al., 2012). A fast onset of action is particularly important for NAL, given its use in emergency medicine and minor surgeries (Narver, 2015). Beyond systemic analgesia, inhaled NAL may also offer local therapeutic benefits in the lungs. For example, NAL demonstrated anti-inflammatory effects on lung macrophages (Zeng et al., 2020) and has been used in patients undergoing thoracoscopic lobectomy to reduce postoperative inflammation (Zhang et al., 2017). It may also relax pulmonary arteries (Sun et al., 2006) and suppress the growth of non-small cell lung cancer cells (while sparing normal epithelial cells) via kappa-opioid receptor activation (Kuzumaki et al., 2012). Recent clinical trials further suggest that NAL may reduce cough in patients with idiopathic pulmonary fibrosis (Maher et al., 2023) and protect the lungs when co-administered with dexmedetomidine by improving oxygenation and reducing pulmonary fluid content (Wang et al., 2022). These emerging therapeutic potentials support the rationale for pulmonary delivery of NAL.

This study aimed to develop inhalable NAL powders using spray drying, with and without the addition of L-leucine (hereafter referred to as leucine) or HSA, which were used as dispersion enhancers and powder stabilisers. Leucine is an endogenous, generally regarded as safe (GRAS) amino acid used as an excipient in inhalable dry powder formulations due to its distinct physicochemical and aerodynamic advantages (Alhajj et al., 2021). Leucine preferentially migrates to the particle surface during spray drying and forms a hydrophobic shell around particles, reducing cohesive forces and improving dispersibility (Ke et al., 2022). Leucine can also produce wrinkled or corrugated particles to enhance lung deposition (Ke et al., 2022). On the other hand, human serum albumin (HSA) is a non-immunogenic and highly biocompatible protein used in clinical settings as an excipient or stabiliser, demonstrating regulatory acceptance (Chow et al., 2019). For example, it has been used in approved injectable formulations, such as Abraxane® and Victoza® (Murphy et al., 2025). Although HSA is an endogenous and abundant protein present in the lungs (Bosquillon et al., 2001), limited human data are available on its inhalation (Todisco et al., 1990) and its potential adverse pulmonary effects remain unknown. Nonetheless, HSA contributes to a more stable powder matrix and optimises particle morphology, and has therefore been used in multiple inhalable powders

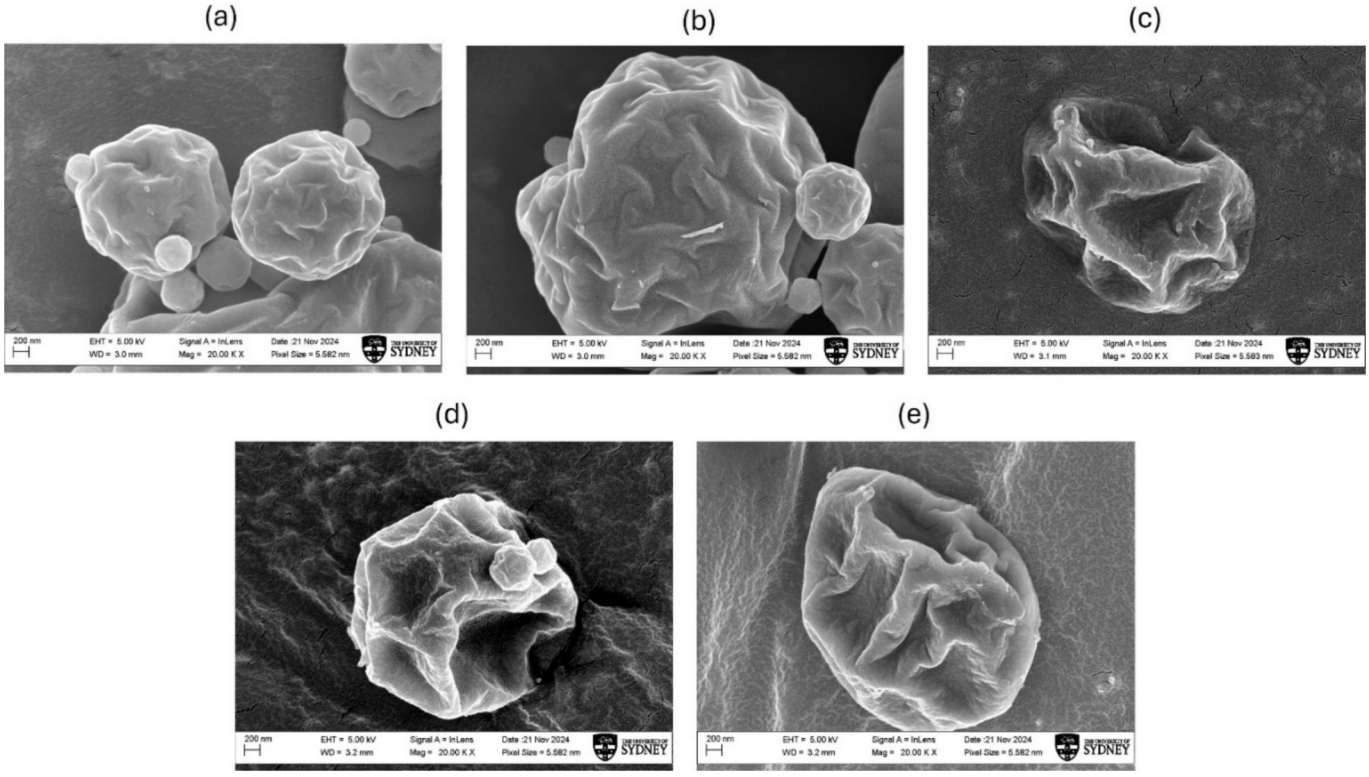

Fig. 1. Scanning electron microscopy images of (a) SD NAL, (b) NAL10L, (c) NAL10HSA, (d) NAL20L, and (e) NAL20HSA.

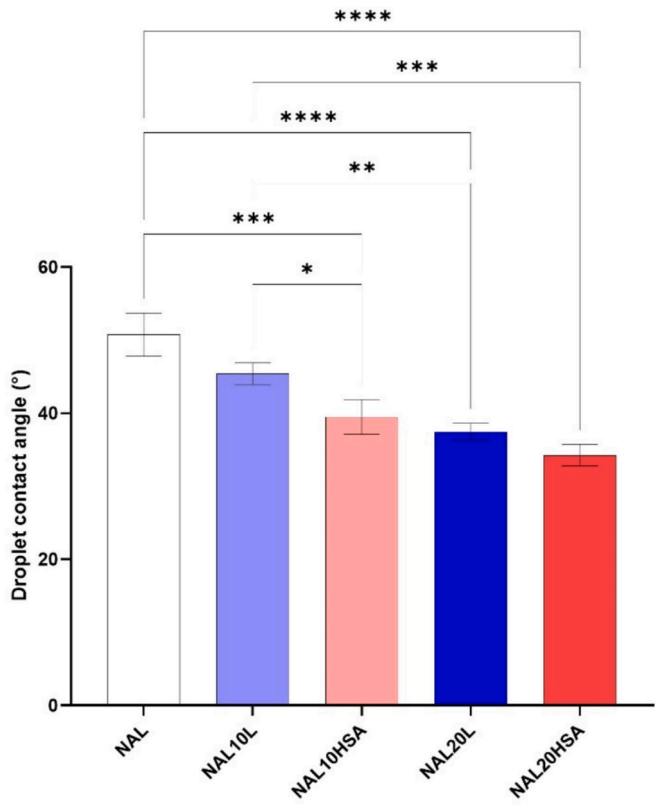

Fig. 2. Droplet contact angles of (a) nalbuphine hydrochloride solution (NAL), (b) nalbuphine hydrochloride + 10 % w/w leucine solution (NAL10L), (c) nalbuphine hydrochloride + 10 % w/w human serum albumin solution (NAL10HSA), (d) nalbuphine hydrochloride + 10 % w/w leucine solution (NAL20L), and (e) nalbuphine hydrochloride + 20 % w/w human serum albumin solution (NAL20HSA).

(Chow et al., 2019; Li et al., 2025; Maa et al., 1997; Seville et al., 2007; Tai et al., 2025). In this study, the physiochemical properties and aerosol performance of the spray dried powders were examined. The one-month storage stability of the most dispersible powder was also assessed.

2. Materials and methods

2.1. Materials

NAL was purchased from PhytoHealth Corporation (Taipei, Taiwan, Republic of China). Leucine, HSA, sodium dihydrogen phosphate, and high-performance liquid chromatography (HPLC) grade acetonitrile were bought from Sigma-Aldrich (St. Louis, United States). A Milli-Q® Direct Water Purification System (Millipore, Massachusetts, United States) was used to obtain ultrapure water (resistivity = 18.2 MΩ·cm).

2.2. Spray drying

Powders (Table 1) were prepared using a Büchi S300 spray dryer coupled with a conventional two-fluid nozzle (BUCHI Labortechnik AG, Flawil, Switzerland). These formulations contained either 10 % w/w or 20 % w/w of leucine (NAL10L or NAL20L) or HSA (NAL10HSA or NAL20HSA) as excipients. NAL was spray dried individually as a control (SD NAL). Feed solutions (16 mg/mL in ultrapure water) were atomised at a feed rate of 4 mL/min, with an inlet temperature of 140 °C, outlet temperature of 70–72 °C, atomising gas flow of 742 L/min, and aspiration rate at 23 m^3/h. The powders were collected into a plastic container inside an acrylic box maintained at relative humidity (RH) < 15 % and stored in a desiccator at 25 ± 2 °C and 30 % RH prior to further use.

2.3. Particle size distribution

The particle size distribution of the powders was measured at 4 bar air pressure using a Mastersizer 3000 with an Aero S dry powder accessory (Malvern Panalytical Ltd., Malvern, United Kingdom). The refractive indices of NAL and leucine were 1.702 and 1.463, respectively. The refractive index of HSA was not reported before, and hence that of bovine serum albumin (1.602) was used instead. For formulations, the refractive indices were calculated based on the mass ratio of each component, as shown in Table 1. Measurements were conducted in triplicate. The reported D_{10}, D_{50}, and D_{90} were the volumetric equivalent diameters at 10 %, 50 %, and 90 % undersize, respectively. The span ($(D_{90}-D_{10})/D_{50}$) were also reported to describe the width of the size distribution.

2.4. Particle morphology

The morphology of spray dried particles was investigated using a scanning electron microscope (SEM; Zeiss Sigma VP HD; Zeiss, Oberkochen, Germany). Samples were spread on the carbon tabs (PELCO®; Ted Pella, California, United States), and then coated with 15 nm of gold using a CCU-010 sputter coater (Safematic, Zizers, Switzerland). Images were acquired at 5 kV beam accelerating voltage and 20,000 x magnification.

2.5. Droplet contact angle

Droplet contact angles were measured using a goniometer (Ramé-Hart instruments, Succasunna, NJ, USA). A 5 μL drop of NAL solution, with and without excipients (leucine or HSA) at a concentration of 16 mg/mL (the same as used for spray drying) was applied onto a glass slide. Image of the droplets was acquired immediately and analysed using ImageJ (Schneider et al., 2012). Triplicate measurements were performed for each sample.

2.6. Optical Photothermal Infrared Spectroscopy (O-PTIR)

The NAL-excipient interactions and the particle surface enrichment of excipients were determined using optical photothermal infrared spectroscopy (O-PTIR). Powders were sprinkled onto calcium fluoride substrates (10 × 0.35 mm; Crystan, Dorset, United Kingdom) and analysed using a mIRage-LS microscope (Photothermal Spectroscopy Corporation, California, USA) equipped with a 40 x all-reflective Cassegrain objective and a silicon photodetector. A HYPERspectra Quantum Cascade Laser (tunable wavelength range: 2990–2700 and 1890 to 790 cm^{-1}), collinear with a continuous-wave visible detection laser (532 nm), was used. The excitation laser was pulsed at 100 kHz with a pulse width of 100 ns to collect the O-PTIR spectra at a spectral resolution of 2 cm^{-1}. The IR and probe beam power was 20 % and 6 %, respectively. O-PTIR spectra for more than 100 particles were averaged followed by second derivative analysis using a five-point Savitzky–Golay smoothing function with a third-order polynomial.

Chemical maps were obtained at wavenumbers specific to NAL (1117 cm^{-1}), leucine (1465 cm^{-1}), and HSA (1542 cm^{-1}) with a step size of 300 nm. Overlaid images of NAL to excipient (leucine or HSA) were used to qualitatively evaluate particle surface enrichment in each sample. All spectral acquisition, image capture, and analysis were performed using PTIR studio 4.0 software (Photothermal Spectroscopy Corporation, California, USA).

2.7. X-ray powder diffraction (XRD)

Powder crystallinity was evaluated using a SmartLAB SE powder diffractometer (Rigaku Corporation, Tokyo, Japan). The powders were

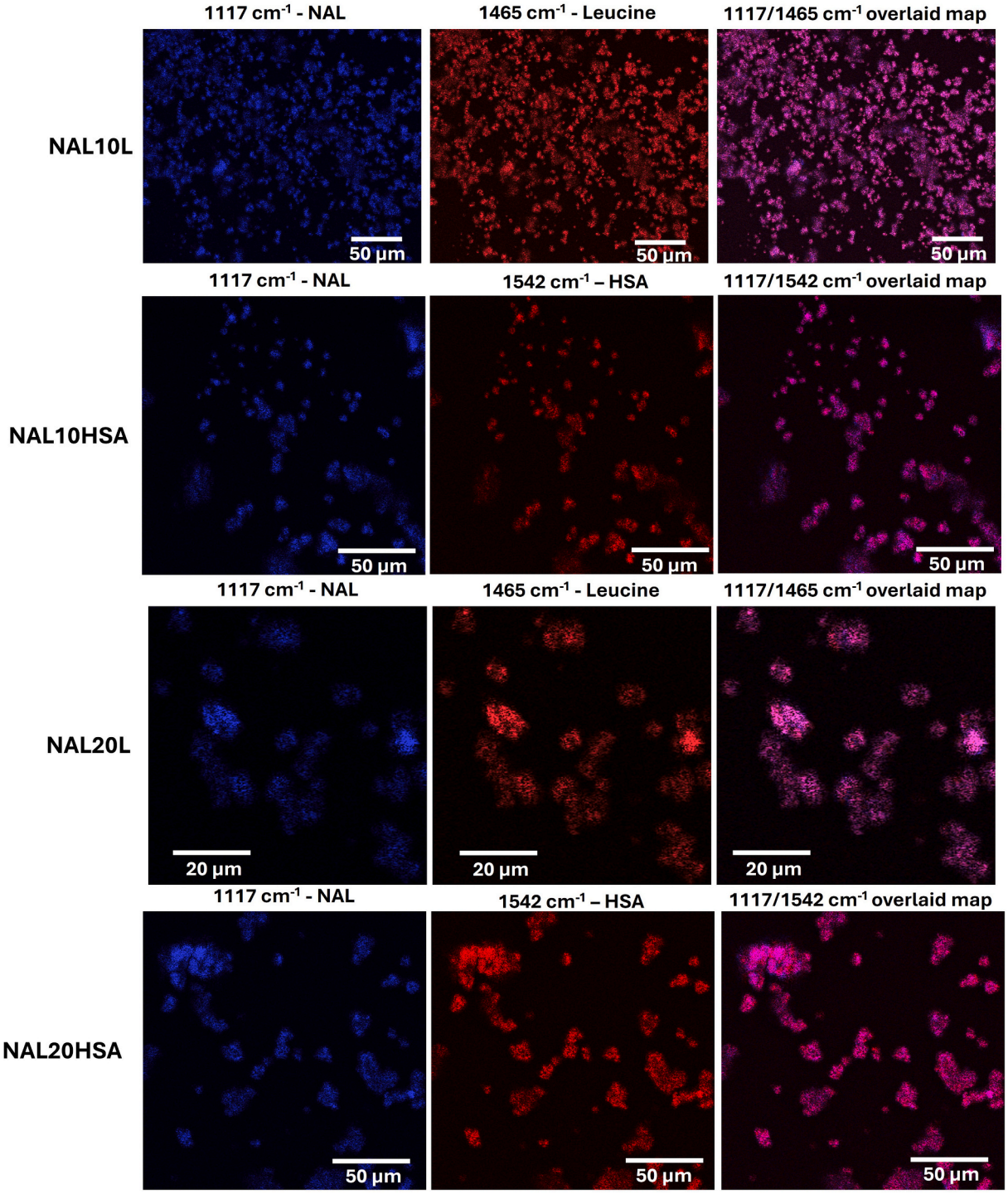

Fig. 3. O-PTIR chemical maps of NAL10L, NAL10HSA, NAL20L, and NAL20HSA. The left panel shows the chemical maps of nalbuphine hydrochloride (NAL) collected at 1117 cm^{-1}. The middle panel depicts the chemical maps of leucine (collected at 1465 cm^{-1}) or human serum albumin (HSA; collected at 1542 cm^{-1}). The right panel presents the overlaid maps of the two corresponding wavenumbers.

first loaded on zero diffraction plates and then subjected to copper Kα radiation at room temperature. The current was 45 mA, while the voltage was 40 kV. The scattered intensity of the samples was recorded from 5 to 50° at a scan speed of 5° per min and step size of 0.01°.

2.8. Thermogravimetric analysis (TGA)

A TGA/DSC 1 with the STARe System (Mettler Toledo, Zürich, Switzerland) was used to determine the residual solvent content in the powders. Approximately 5 mg powders were weighed in an open alumina crucible and heated from 25-160 °C at a constant heat rate of 10 °C/min under 20 mL/min nitrogen flow. The mass change of the powder was recorded.

2.9. Differential scanning calorimetry (DSC)

The thermal events of the spray dried powders were determined using a differential scanning calorimeter (DSC 1 model with the STARe

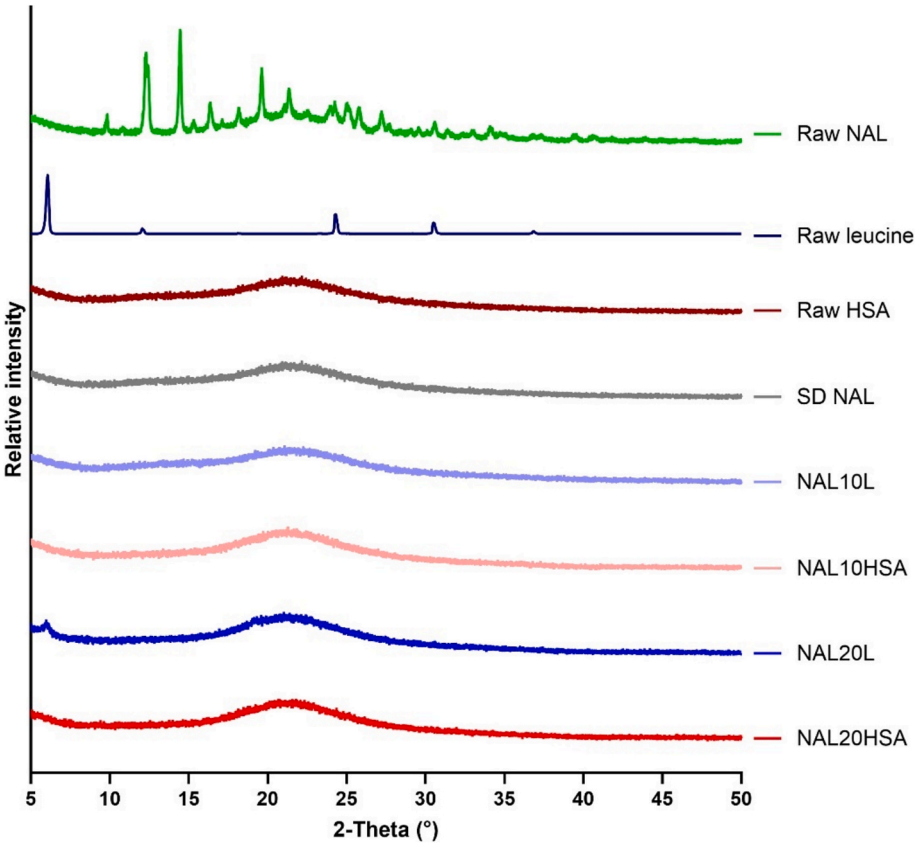

Fig. 4. X-ray powder diffraction patterns of raw materials and spray dried powders containing nalbuphine hydrochloride (NAL), leucine, and human serum albumin (HSA).

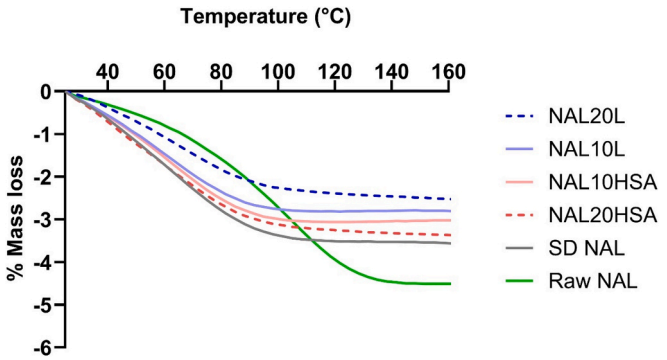

Fig. 5. Thermogravimetric analysis of raw materials and spray dried powders containing nalbuphine hydrochloride (NAL), leucine, and human serum albumin (HSA).

System; Mettler Toledo, Zürich, Switzerland). Aluminium pans loaded with about 5 mg samples were crimp-sealed with lids with pinhole. The thermograms were obtained by heating the samples from 25 to 350 °C at a constant rate of 10 °C/min under 20 mL/min nitrogen flow.

2.10. Dynamic vapour sorption (DVS)

The moisture sorption–desorption profiles of the powders were obtained using dynamic vapour sorption (DVS; DVS-Intrinsic, Surface Measurement Systems, London, United Kingdom). Approximately 10 mg powder was equilibrated in the chamber at 25 °C/0% RH under continuous nitrogen flow. It was then subjected to two adsorption–desorption cycles from 0-90 % RH. RH was increased in 10 % increments, with the equilibrium moisture content criterion of each step at ≤0.002 % per min.

2.11. Density measurement

The bulk densities (ρ_b) of the formulations were measured by accurately weighing 1–2 cm3 of powder in a 10 cm3 graduated cylinder. The powder in the cylinder was then tapped approximately 1200 times using a tapping apparatus (Surface Measurement Systems Ltd, London, United Kingdom) and the final volume was recorded to determine the tapped density (ρ_t). Triplicate measurements were performed for all samples. The flowability of the powders was assessed by calculating Carr's index using Equation (1).

$$Carr's\ index = \frac{(\rho_t - \rho_b)}{\rho_t} \times 100 \quad (1)$$

2.12. Aerosol performance

The aerosol performance of the spray dried powders was examined using the Next Generation Impactor (NGI; Copley, Nottingham, United Kingdom) with the United States Pharmacopeia throat. Prior to dispersion, the collection cups inside the NGI were coated with a thin layer of silicone (Slipicone, Victoria, Australia) to avoid particle bounce. Powder (20 ± 2 mg) was filled into a size 3 hydroxypropyl methylcellulose capsule (Capsugel, Sydney, Australia) and dispersed using a high resistance RS01 inhaler (Plastiape S.p.A., Osnago, Italy). This device was selected because it is an approved dry powder inhaler for therapeutic use (not diagnostic testing) and requires only moderate inhalation effort from patients to achieve sufficient lung deposition at a low airflow rate (50–70 L/min), which also helps reduce oropharyngeal deposition (Yang et al., 2016). The inhaler was connected to the throat with a

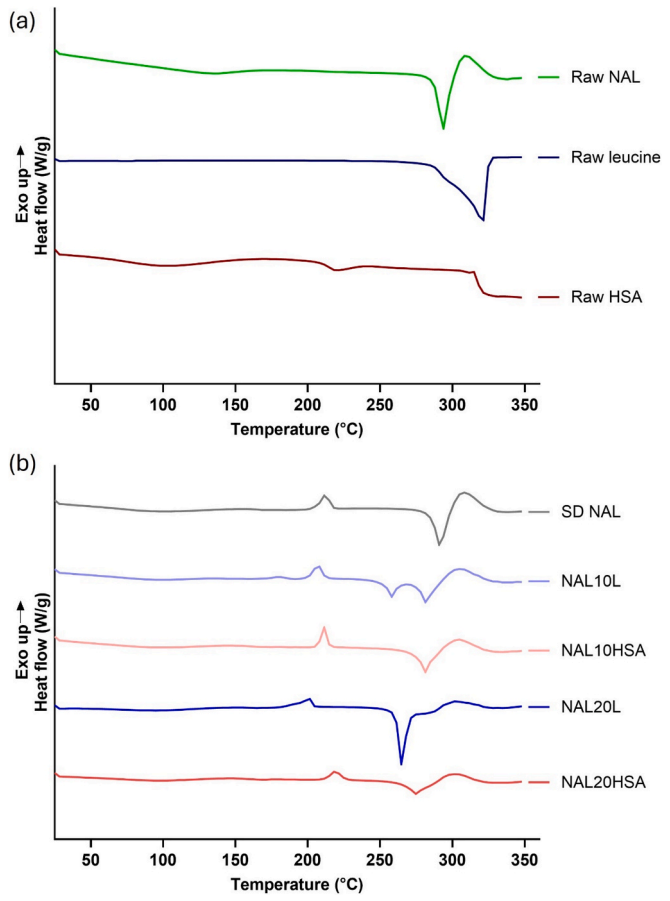

Fig. 6. Differential scanning calorimetry thermograms of (a) raw materials and (b) spray dried powders containing nalbuphine hydrochloride (NAL), leucine, and human serum albumin (HSA).

Table 3
Thermal events (in °C) of raw materials and spray dried powders containing nalbuphine hydrochloride (NAL), leucine, and human serum albumin (HSA).

Formulations	Crystallisation	Sublimation	Melting	Decomposition
Raw NAL	/	/	293.8	308.3
Raw leucine	/	319.3	/	/
Raw HSA	/	/	/	/
SD NAL	211.8	/	290.5	308.5
NAL10L	208.4	257.7	280.9	305.0
NAL10HSA	211.8	/	281.0	304.9
NAL20L	201.7	/	263.8	301.7
NAL20HSA	218.3	/	274.6	301.6

silicone adapter. The dispersion was conducted at 4 kPa pressure drop (equivalent to 57 L/min). The aerodynamic cut-off diameters of the NGI stages (from Stages 1 to 8) are >8.29, 8.29, 4.58, 2.89, 1.70, 0.97, 0.57, and 0.35 μm. The duration of dispersion was 4.3 s, allowing 4 L of air to pass through the inhaler. The drug deposited on the capsule, inhaler, adapter, throat, and the NGI stages was rinsed with 5 mL ultrapure water and quantified by HPLC. Triplicate dispersions were conducted for each formulation. Emitted fraction (EF), fine particle fractions (FPFs) <5 μm and <3 μm, mass median aerodynamic diameter (MMAD), and geometric standard deviation (GSD) were calculated. The EF was the percentage of emitted dose (sum of mass deposited on adaptor, throat, and the NGI stages) with respect to the recovered dose. The FPFs were defined as the percentages of fine particle doses (<5 μm and <3 μm) relative to the recovered dose. The aerodynamic diameter that split the aerodynamic particle size distribution in half by mass was the MMAD. The ratio between the MMAD and the aerodynamic diameter at 16 % undersize was defined as the GSD.

2.13. Stability test

Stability test was conducted using the formulation with the best aerosol performance (i.e. the highest FPFs). It was stored as a loose powder in a plastic container and directly exposed at 25 °C/30 % RH (as a control) and 25 °C/60 % RH for one month. After storage, the aerosol performance of the powder was re-evaluated using the same method described in Section 2.9.

2.14. Drug quantification

NAL was quantified with a HPLC system consisting of a Shimadzu CBM-20A controller, a LC-20AT pump, a SIL-20A HT autosampler, a SPD-20A UV/VIS detector, and a Waters Nova-Pak C18 column (4 μm; 150 × 3.90 mm). The mobile phase was 70:30 v/v 0.05 M sodium dihydrogen phosphate buffer (pH 3.5):acetonitrile, constantly flowing at 1 mL/min. The UV detection wavelength was 230 nm. The standard solutions were prepared in ultrapure water by serial dilution. The calibration curves were linear over the concentration range of 3.9 – 1000 μg/mL ($r^2 > 0.99$).

2.15. Statistical analysis

Data was analysed using one-way analysis of variance (ANOVA) followed by Tukey's *post hoc* test. Differences were considered statistically significant with a $p < 0.05$ and $\alpha < 0.05$.

3. Results

The production yields of the spray dried powders were 80–85 %, as shown in Table 2. The D_{50} of the particles in all formulations were below 4 μm, with span values about 2 (Table 2). SEM images showed that SD NAL particles were corrugated (Fig. 1a), while those containing leucine or HSA appeared more wrinkled (Figs. 1b–e). The surface of NAL20L appeared rougher than that of NAL10L (Figs. 1b and d), whereas the surfaces of NAL10HSA and NAL20HSA were similar (Figs. 1c and e).

Fig. 2 shows the droplet contact angle of the NAL and excipient-containing solutions. The contact angles of NAL solution (50.8 ± 3.0°) and NAL10L solution (45.4 ± 1.5°) were comparable. Both were significantly larger than those of NAL10HSA (39.5 ± 2.4°), NAL20L (37.5 ± 1.2°), and NAL20HSA (34.3 ± 1.5°), which were comparable to each other.

Chemical maps (Fig. 3) collected from spray-dried NAL particles containing either leucine or HSA at specific wavenumbers—1117 cm^{-1} (NAL, C–O stretching), 1465 cm^{-1} (leucine, CH_2 bending), and 1542 cm^{-1} (HSA, N–H bending)—confirmed the homogeneous distribution of both NAL and the excipients. The overlaid chemical maps of NAL with either leucine or HSA showed a pink coloration, indicating the overlap of blue (excipient) and red (NAL) signals, which suggests surface enrichment of the particles with the respective excipient. However, depending on the concentration of leucine or HSA, faint blue regions were still visible, indicating areas with lower NAL presence. In the overlaid map of NAL20L, particles exhibited more red and pink clusters compared to NAL10L, suggesting greater surface coverage at higher leucine concentrations. A similar trend was observed between NAL10HSA and NAL20HSA. At equivalent mass concentrations, HSA appeared to provide more extensive surface coverage than leucine.

Raw NAL and leucine were crystalline, as evidenced by their distinct peaks in the X-ray diffractograms in Fig. 4. In contrast, raw HSA showed a halo pattern, indicating its amorphous nature. Similarly, all spray dried formulations also showed halo patterns (Fig. 4), confirming their amorphous state. However, a faint peak at 6° was observed in NAL20L.

TGA results are depicted in Fig. 5. Raw NAL contained 4.5 % residual

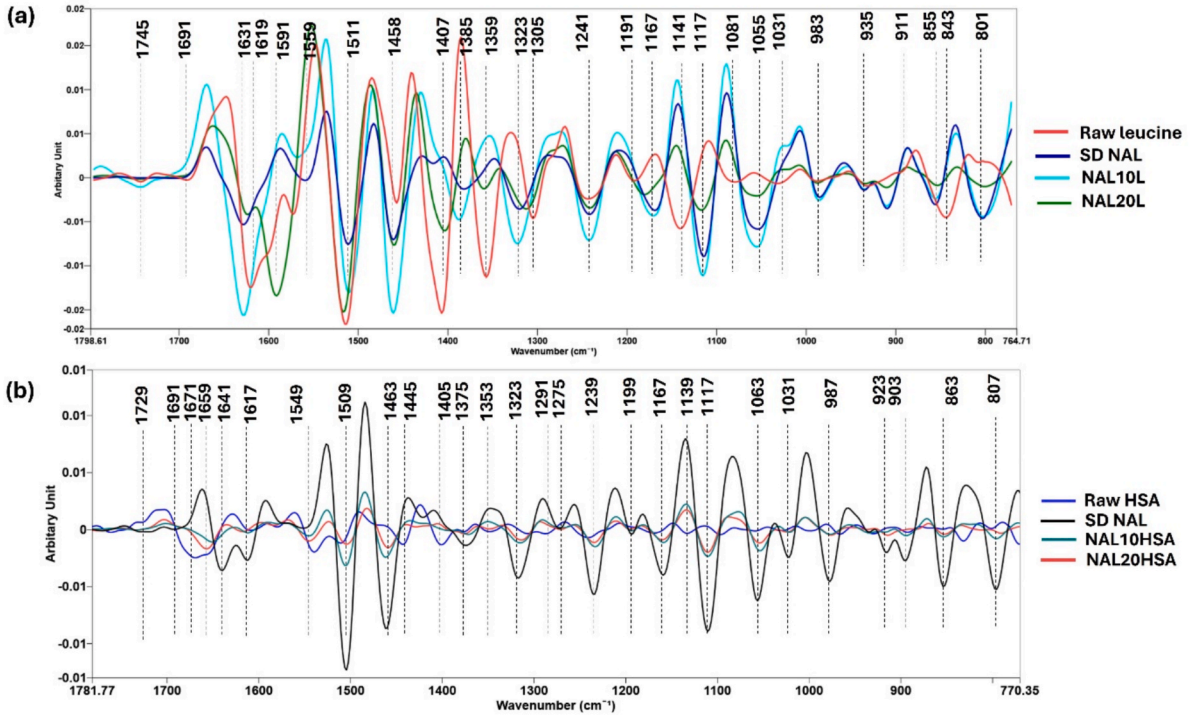

Fig. 7. O-PTIR spectra of (a) raw leucine, SD NAL, NAL10L, and NAL20L and (b) raw human serum albumin (HSA), SD NAL, NAL10HSA, and NAL20HSA.

solvent. Spray drying reduced this to 3.6 % in SD NAL. The addition of HSA slightly decreased the residual solvent content to 3.0–3.4 %, while leucine reduced it further to 2.5–2.8 % (Fig. 5).

Fig. 6a shows the DSC results of the raw materials. No thermal event was observed for raw HSA. Raw leucine displayed an endothermic peak beginning at 284.8 °C (Fig. 6a), indicating decomposition (Pokorný et al., 2020). Raw NAL showed an endothermic melting peak at 293.8 °C followed by an exothermic decomposition peak at 308.3 °C (Fig. 6a) (Hanko and Vlahova, 2011). These thermal events were also observed in the spray dried powders, with melting between 263.8–290.5 °C and decomposition between 301.7–308.5 °C (Fig. 6b; Table 3). An exothermic event between 208.4–218.3 °C was present in all formulations (Fig. 6b; Table 3), corresponding to crystallisation from the amorphous state. NAL10L also exhibited an additional endothermic peak at 257.7 °C, indicating leucine sublimation (Li et al., 2016), which was not observed in NAL20L (Fig. 6b; Table 3).

The O-PTIR spectra of the raw materials and formulations are shown in Fig. 7. SD NAL exhibited peaks at 1559 (C-N stretching), 1385, 1323 (–CH_2 wagging), 1463 (CH_2 bending), and 1167 cm^{-1} (C-O stretching) (Khanna et al., 2025; Mestek, 2025). Similar peaks at 1385, 1323, and 1167 cm^{-1} were also observed in NAL10L, but the peak at 1559 cm^{-1} was shifted to 1564 cm^{-1}. Additional peak shifts were found in NAL20L, including from 1323 to 1305 cm^{-1} and from 1167 to 1191 cm^{-1}. While the peak at 1385 cm^{-1} disappeared in the spectrum of NAL20L, new peaks emerged at 1407, 1591, and 1359 cm^{-1}. On the other hand, for NAL10HSA and NAL20HSA, the peaks around 1664 cm^{-1} (amide I band of HSA) shifted toward 1641 cm^{-1} with decreasing HSA content. New peaks appeared at 1063 and 1031 cm^{-1} in both NAL10HSA and NAL20HSA spectra. A decrease in peak intensity with increasing HSA content was observed at multiple wavenumbers, including 1509, 1375, and 1115 cm^{-1}.

Moisture sorption profiles showed that SD NAL adsorbed 14 % w/w moisture at 80 % RH, with a sharp mass loss (Fig. 8a). Similar behaviour was observed in NAL10L (12 %), NAL20L (11 %), and NAL10HSA (16 %) (Figs. 8b–d). NAL10L also showed a slight mass decrease at 60 % RH, suggesting leucine recrystallisation. In NAL20HSA, recrystallisation occurred at 90 % RH after adsorbing 18 % w/w moisture (Fig. 8e). Upon desorption, SD NAL retained 8 % w/w more mass than baseline (Fig. 8a), close to the theoretical water content (8.38 % w/w) required for complete transformation to the dihydrate form. The other recrystallised powders retained only 6–7 % moisture (Figs. 8b–e), indicating partial transformation.

Table 4 presents the bulk and tapped densities of the spray dried powders. The bulk and tapped densities of SD NAL was 0.2 ± 0.0 and 0.3 ± 0.0 g/cm^3, respectively. The addition of 10 % w/w leucine to the formulation increased the bulk density (0.3 ± 0.0 g/cm^3) but did not affect the tapped density, which remained at 0.3 ± 0.0 g/cm^3. For NAL20L, both bulk and tapped densities increased to 0.3 ± 0.0 and 0.5 ± 0.0 g/cm^3, respectively. In contrast, the addition of 10 % and 20 % w/w HSA decreased the bulk density to 0.1 ± 0.0 g/cm^3 and tapped density to 0.2 ± 0.0 g/cm^3. The Carr's index of SD NAL was 14.5 ± 4.3 %, indicating good flowability (Seville et al., 2007). NAL10L exhibited the lowest Carr's index at 4.1 ± 2.1 %, classifying it as a powder with excellent flowability (Seville et al., 2007). However, NAL10HSA, NAL20L, and NAL20HSA had Carr's index values of 36.8 ± 2.6 %, 41.0 ± 2.8 %, and 27.9 ± 4.6 %, respectively, suggesting poor flowability (Seville et al., 2007).

The aerodynamic particle size distributions of the spray dried powders are illustrated in Fig. 9. SD NAL showed the highest drug retention in the capsule and inhaler, as well as throat deposition. These were reduced by adding 10 % or 20 % (w/w) of either leucine or HSA, with greater improvements observed at 20 % (Fig. 9). Leucine was more effective than HSA at the same mass concentration, resulting in less retention and more drug deposition in the later NGI stages (Fig. 9). The MMADs of SD NAL (2.9 ± 0.2 μm) and NAL20L (3.1 ± 0.2 μm) were comparable and significantly smaller than those of NAL10L (3.7 ± 0.2 μm), NAL10HSA (3.9 ± 0.1 μm), and NAL20HSA (4.0 ± 0.0 μm). The GSD values of SD NAL (2.1 ± 0.0), NAL10HSA (2.1 ± 0.0), and NAL20HSA (2.0 ± 0.0) were comparable, and all were significantly lower than those of NAL10L (2.7 ± 0.3) and NAL20L (4.5 ± 0.3), with the difference between the two leucine formulations also being significant.

The EF of SD NAL was 78.4 ± 0.7 %, which was significantly lower than those of the other four formulations (Fig. 10). While comparable

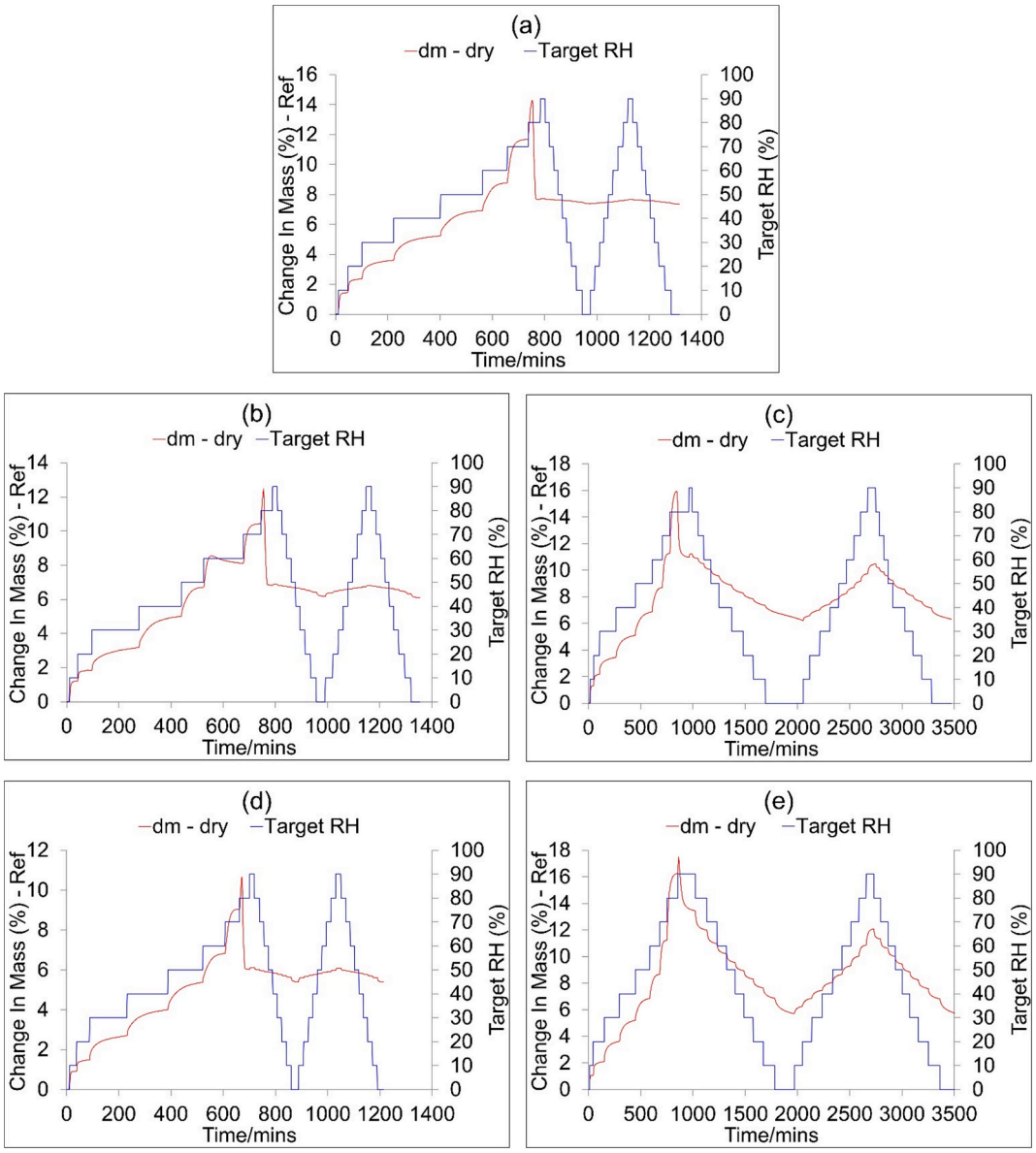

Fig. 8. Moisture sorption profiles of (a) SD NAL, (b) NAL10L, (c) NAL10HSA, (d) NAL20L, and (e) NAL20HSA.

Table 4
The bulk and tapped densities and Carr's index of the spray dried powders.

Formulations	Bulk density (g/cm^3)	Tapped density (g/cm^3)	Carr's index (%)
SD NAL	0.2 ± 0.0	0.3 ± 0.0	14.5 ± 4.3
NAL10L	0.3 ± 0.0	0.3 ± 0.0	4.1 ± 2.2
NAL10HSA	0.1 ± 0.0	0.2 ± 0.0	36.8 ± 2.6
NAL20L	0.3 ± 0.0	0.5 ± 0.0	41.0 ± 2.8
NAL20HSA	0.1 ± 0.0	0.2 ± 0.0	27.9 ± 4.6

EFs were observed in NAL20L (91.5 ± 2.1 %) and NAL20HSA (91.3 ± 0.5 %), they were significantly higher than those of NAL10L (87.1 ± 1.2 %) and NAL10HSA (86.4 ± 1.9 %) (Fig. 10). For FPD and FPF <5 μm, the lowest ones were from SD NAL (4780.9 ± 412.8 μg/24.8 ± 1.4 %; Fig. 11a and Fig. 12a). Adding 10 % or 20 % w/w leucine or HSA significantly improved the FPDs and FPFs < 5 μm. Comparable FPDs and FPFs < 5 μm were observed from NAL10HSA (6258.7 ± 302.5 μg/32.8 ± 1.5 %; Fig. 11a and Fig. 12a) and NAL20HSA (6258.7 ± 302.5 μg/37.0 ± 1.8 %; Fig. 11a and Fig. 12a), while NAL10L (7636.6 ± 576.7 μg/39.2 ± 3.5 %; Fig. 11a and Fig. 12a) and NAL20L (7683.6 ± 344.0 μg/47.5 ± 4.1 %; Fig. 11a and Fig. 12a) had comparable, but higher FPDs and FPFs. The FPF < 5 μm of NAL20L (47.5 ± 4.1 %) was significantly higher than that of NAL10L (39.2 ± 3.5 %). Furthermore, NAL10L exhibited significantly higher FPD and FPF than NAL10HSA. Although NAL10L had a significantly higher FPD than NAL20HSA, their FPFs were comparable. Both FPD and FPF of NAL20HSA were significantly lower than those of NAL20L. On the other hand, the FPDs and FPFs < 3 μm of SD NAL (3151.1 ± 146.9 μg/16.4 ± 0.3 %; Fig. 11b and Fig. 12b), NAL10HSA (3146.1 ± 233.9 μg/16.5 ± 1.3 %; Fig. 11b and Fig. 12b), and NAL20HSA (3365.4 ± 273.9 μg/18.9 ± 1.1 %; Fig. 11b and Fig. 12b) were comparable. In contrast, the addition of 10 % and 20 % w/w leucine significantly increased the FPDs/FPFs < 3 μm to 4270.9 ± 454.1 μg/22.0 ± 2.7 % and 5128.4 ± 144.6 μg/31.7 ± 2.2 %, respectively (Fig. 11b and Fig. 12b). Notably, the FPD < 3 μm of NAL10L was already significantly higher than those of the HSA-containing formulations.

Fig. 13 shows the aerodynamic particle size distribution of NAL20L after one month of storage at 25 °C/30 % RH and 25 °C/60 % RH. The drug recovery was close to 100 % and no additional peaks were observed

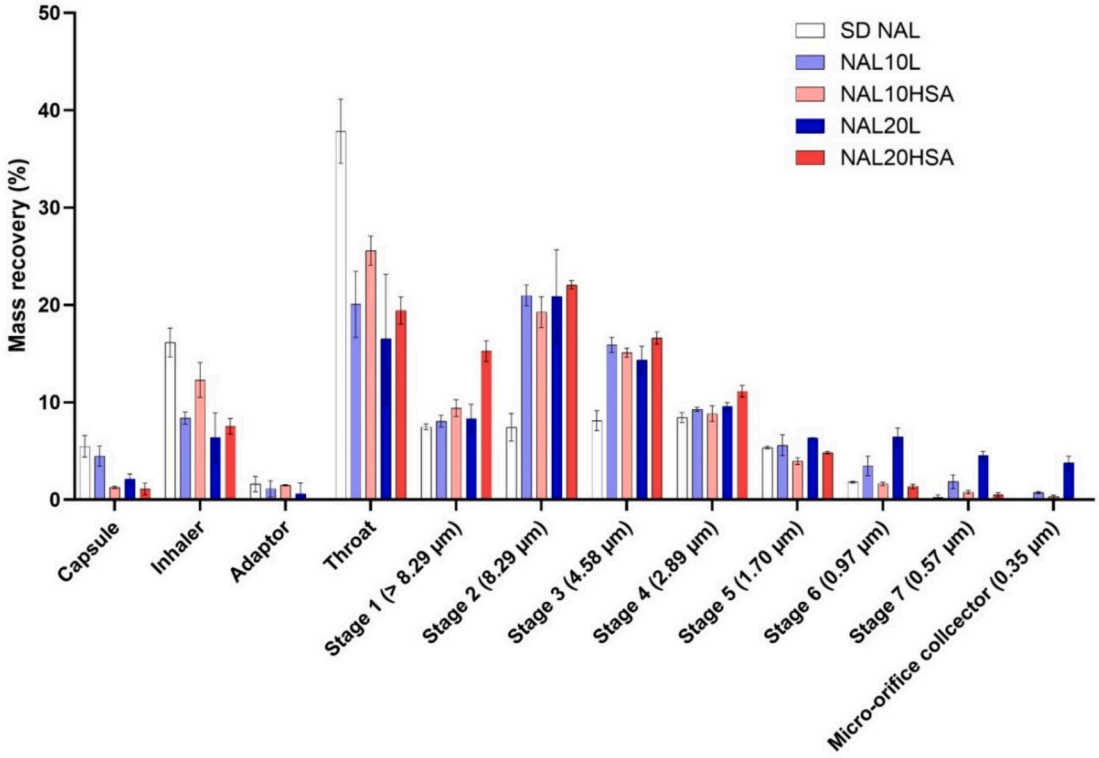

Fig. 9. Aerodynamic particle size distributions of spray dried powders containing nalbuphine hydrochloride (NAL), leucine, and human serum albumin (HSA). Data presented as mean ± standard deviation ($n = 3$).

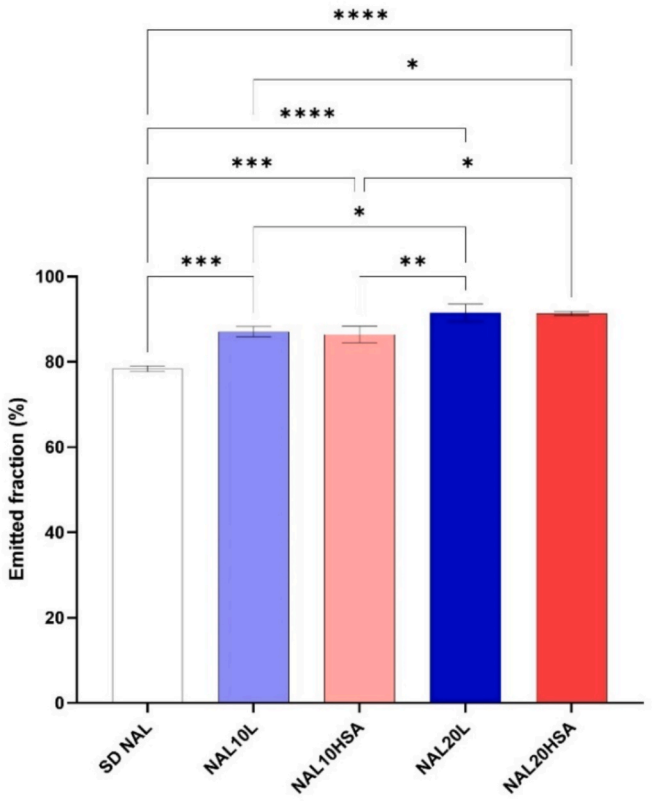

Fig. 10. Emitted fractions of spray dried powders containing nalbuphine hydrochloride (NAL), leucine, and human serum albumin (HSA). Data presented as mean ± standard deviation ($n = 3$; *$p \leq 0.05$; **$p \leq 0.01$; ***$p \leq 0.001$; ****$p \leq 0.0001$).

in the HPLC chromatograms, indicating the chemical stability. The aerodynamic particle size distributions were comparable under both conditions (Fig. 10), suggesting good physical stability. This was further supported by the consistent FPFs < 5 μm/< 3 μm at 25 °C/30 % RH (47.9 ± 2.3 %/32.1 ± 1.3 %; Fig. 13) and 25 °C/60 % RH (46.9 ± 0.8 %/34.9 ± 0.7 %; Fig. 13).

4. Discussion

Inhaled opioids have previously been investigated in human PK studies, demonstrating highly promising profiles. For example, the bioavailability of inhaled fentanyl was about 100 % and its time to reach peak concentration was comparable to that of intravenous injection (Macleod et al., 2012). Both intravenous opioids and inhaled fentanyl also provided similar analgesic efficacy (Thompson and Thompson, 2016). Another example is inhaled morphine, which exhibited a 59–100 % bioavailability and a comparable time to reach peak concentration as intravenous infusion (Dershwitz et al., 2000; Ward et al., 1997). These findings suggest that pulmonary delivery is an efficient and non-invasive route for administering opioids. However, these studies employed either a nebuliser (using a liquid formulation) (Thompson and Thompson, 2016), a soft mist inhaler (Ward et al., 1997), or a flow-independent condensation aerosol inhaler (Staccato® with a drug-only formulation as a thin film coated on a substrate for heating) (Macleod et al., 2012), and none have investigated the use of dry powder inhalers. Therefore, the current study is the first to develop inhalable opioid powders. While multiple opioids are available, NAL was formulated in this study due to its widespread clinical use and better safety profile compared to other opioids.

In this study, NAL powders were produced via spray drying, which is a rapid, reproducible, and scalable one-step process (Marante et al., 2020). The high feasibility of this method was demonstrated by the good production yields at 80–85 %. The spray dried particles were physically small (3–4 μm; Table 2) and exhibited a corrugated surface, as shown in

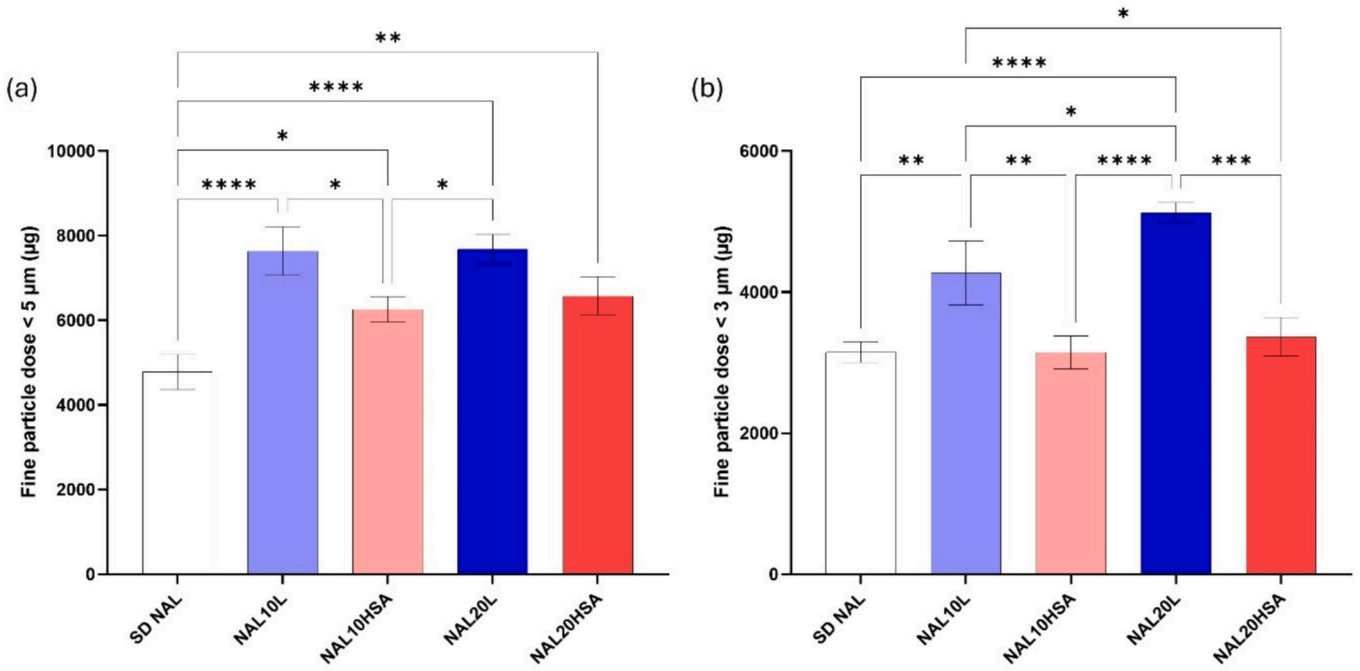

Fig. 11. (a) Fine particle dose < 5 μm and (b) fine particle dose < 3 μm of spray dried powders containing nalbuphine hydrochloride (NAL), leucine, and human serum albumin (HSA). Data presented as mean ± standard deviation ((n = 3; *p ≤ 0.05; **p ≤ 0.01; ***p ≤ 0.001; ****p ≤ 0.0001).

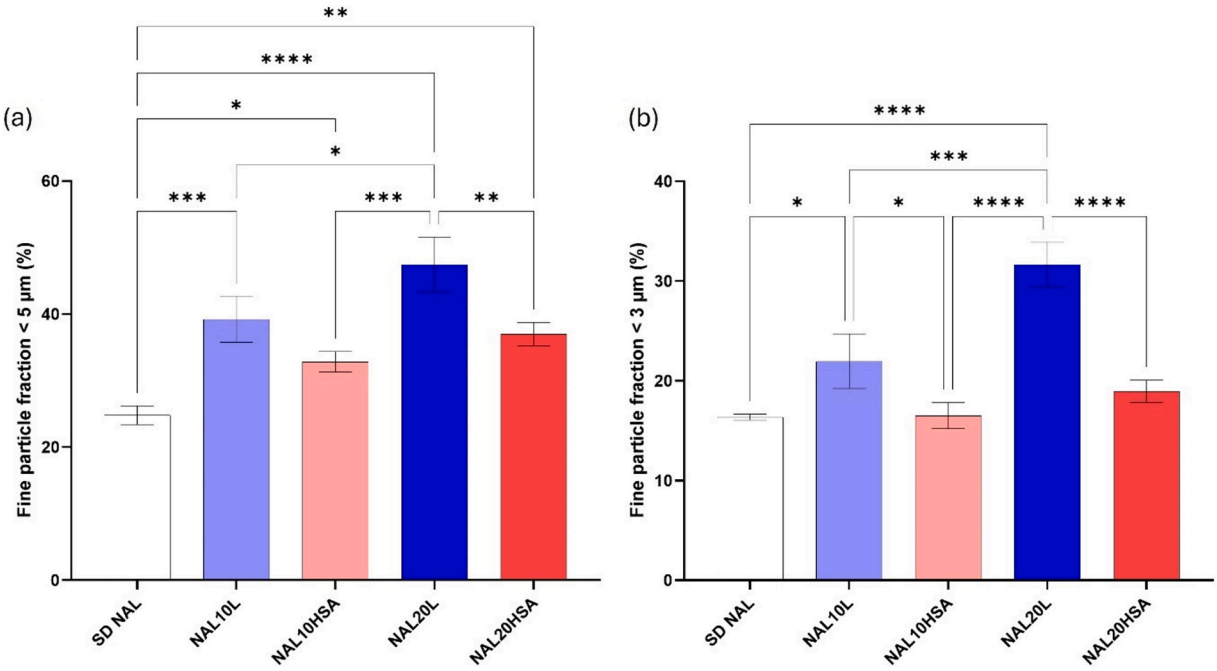

Fig. 12. (a) Fine particle fraction < 5 μm and (b) fine particle fraction < 3 μm of spray dried powders containing nalbuphine hydrochloride (NAL), leucine, and human serum albumin (HSA). Data presented as mean ± standard deviation ((n = 3; *p ≤ 0.05; **p ≤ 0.01; ***p ≤ 0.001; ****p ≤ 0.0001).

the SEM images in Fig. 1. Although SD NAL already displayed surface corrugation, the addition of leucine and HSA further increased surface roughness. Leucine is a hydrophobic amino acid with weak surfactant properties (Chang and Chan, 2022). It is also more hydrophobic than NAL, as indicated by its lower aqueous solubility (22 mg/mL at 25 °C) compared to that of NAL (35.5 mg/mL) (Ordoubadi et al., 2023; Pfizer, 2025). These characteristics enable leucine to accumulate at the droplet surface during spray drying, where it reaches supersaturation, precipitates, and forms a hydrophobic shell (Ke et al., 2022). This shell shrinks with water evaporation to form corrugated particles (Ke et al., 2022). For HSA, it occupies the particle surface as its high molecular weight limits its diffusion during spray drying. When spray drying at a high temperature (i.e. 140 °C in the current study), rapid water evaporation induces formation of a crust on the particle which collapses and causes surface wrinkling (Maa et al., 1997). The effects of HSA and leucine on the droplet and particle surfaces were confirmed by the droplet contact angle measurements and the O-PTIR chemical maps. The surface activity of leucine and HSA in the droplet was demonstrated by a

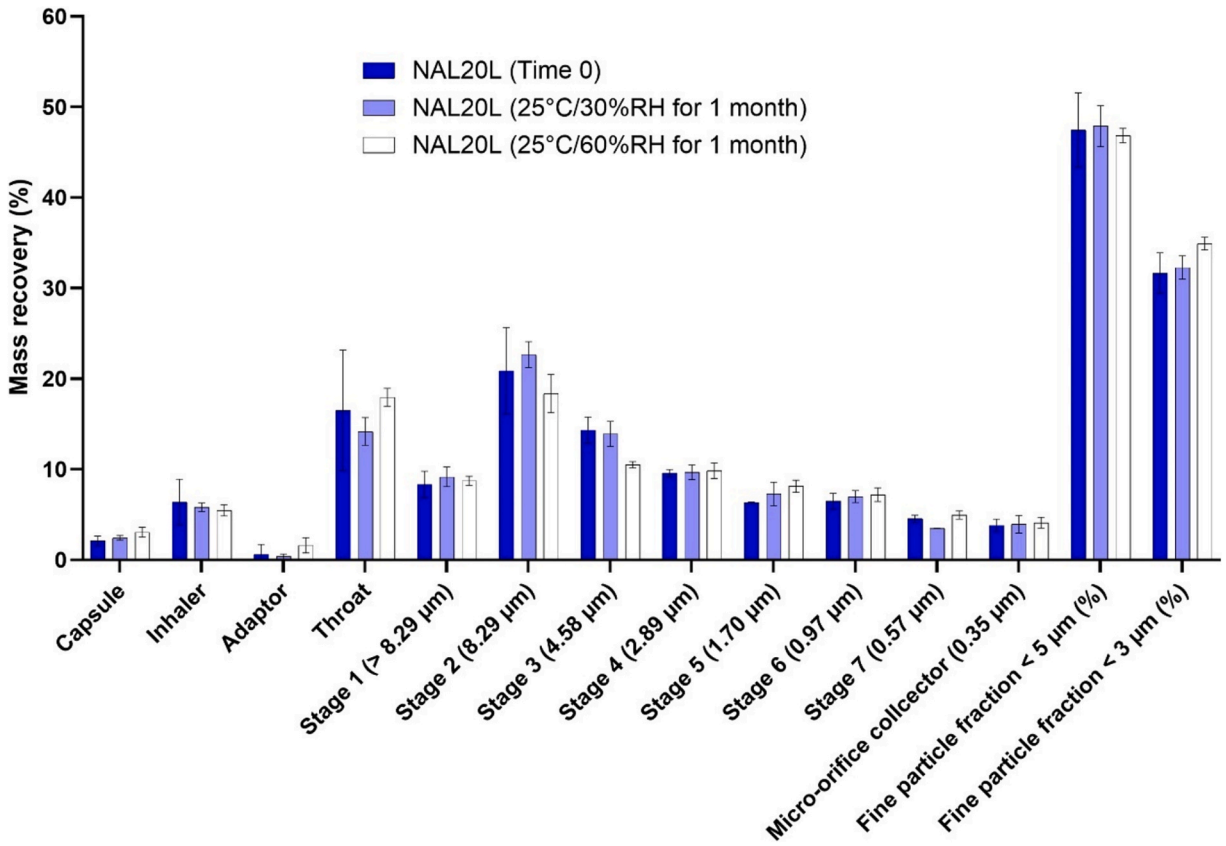

Fig. 13. Aerodynamic particle size distributions, fine particle fraction <5 μm, and fine particle fraction <3 μm of NAL20L after one month of storage at 25 °C under both 30 % and 60 % relative humidity. Data presented as mean ± standard deviation ($n = 3$).

significant decrease of contact angle compared to that of the NAL solution (Fig. 2), indicating their accumulation at the gas-liquid interface. The larger droplet contact angle observed for the NAL solution containing leucine, compared to that containing HSA, suggested that leucine had lower surface activity and was a weaker surfactant, potentially due to its limited amphiphilic nature. After spray drying, the particle surfaces were enriched with leucine or HSA, as evidenced by slight peak shifts and reduced intensities in multiple spectral peaks, as well as the dominance of pink to red colours in the ratio maps (Fig. 3). Traces of faint blue observed in the ratio maps indicated incomplete surface coverage. Increasing the mass concentration of excipients from 10 % to 20 % w/w enhanced the redness of the chemical maps and reduced the presence of blue, suggesting that 20 % w/w excipient resulted in larger surface coverage of the particles.

All spray dried NAL powders were amorphous (Fig. 4) and contained <4 % residual solvent by mass (Fig. 5), indicating efficient drying during production. Since the spray dried formulations were amorphous, their DSC thermograms in Fig. 6 differed from that of the crystalline raw NAL, which only showed an endothermic melting peak at 293.8 °C, followed by an exothermic decomposition peak at 308.3 °C. These results are consistent with previous observations (Hanko and Vlahova, 2011). In contrast, the amorphous spray dried powders first crystallised (as indicated by exothermic events at 208.4–218.3 °C; Table 3), then melted and decomposed (with endothermic melting events at 263.8–290.5 °C, followed by exothermic decomposition event at 301.7–308.5 °C). The addition of excipients influenced the crystallisation temperature and subsequently the melting point of NAL. While SD NAL, NAL10L, and NAL10HSA crystallised at similar temperatures (208.4–211.8 °C), crystallisation occurred earlier for NAL20L (at 201.7 °C) and later for NAL20HSA (at 218.3 °C). These shifts in crystallisation peaks suggest potential molecular interactions between NAL and either leucine or HSA. Such interactions may have affected the packing of NAL crystals, as reflected in the corresponding changings in melting points across formulations. Similar molecular interactions have also been reported in other co-spray dried formulations, such as ciprofloxacin with tryptophan (Chang et al., 2022) and budesonide with arginine (Lu et al., 2019). In this study, the intermolecular interactions between NAL and excipients were supported by peak shifts, peak disappearance, and the emergence of new peaks in the O-PTIR spectra of the formulations (Fig. 7). For NAL10L and NAL20L, the spectral changes suggested the formation of hydrogen bonds or ionic interactions between leucine and NAL. The slight shift of the peak from 1559 to 1564 cm^{-1} in NAL10L indicated a weak hydrogen bond involving the protonated tertiary amine of NAL and the amino or carboxyl group of leucine. Increasing leucine content led to potentially stronger hydrogen bonds, as shown by the significant shift of the peak from 1323 to 1305 cm^{-1} and 1167 to 1191 cm^{-1} in NAL20L, corresponding to CH_2 wagging and C-O stretching, respectively (Mestek, 2025). The C-O shift might originate from the formation of hydrogen bonds between the phenolic hydroxyl group of NAL and the amino group of leucine. The appearance of new peaks at 1591, 1407, and 1359 cm^{-1}, was assigned to the C=C aromatic shift, COO– symmetric stretch, and C-N stretch, respectively (Mestek, 2025). These further supported the formation of ionic interactions. The disappearance of the peak at 1385 cm^{-1} suggested potential steric hindrance by leucine. Similarly, increasing HSA content in the formulations led to potentially stronger hydrogen bonding and conformational changes of HSA. This was evidenced by the peak shift from 1641 to 1664 cm^{-1}, corresponding to the amide I band of HSA. The new peaks at 1063 and 1031 cm^{-1} were attributed to C-O and C-N vibrations, suggesting potential interactions between NAL and HSA side chains (Mestek, 2025). The decreased intensity of peaks at 1509, 1375, and 1115 cm^{-1} indicated the binding of NAL within the HSA binding pockets, resulting in the shielding of NAL functional groups.

Although amorphous powders can enhance drug dissolution and

bioavailability (Bhujbal et al., 2021), they are also prone to recrystallisation, particularly in hygroscopic compounds. SD NAL is moderately hygroscopic as it absorbed about 14 % w/w moisture at 25 °C/80 % RH before undergoing recrystallisation, as shown in Fig. 8 (Newman et al., 2008). While the addition of leucine in NAL10L and NAL20L did not delay recrystallisation, it reduced moisture uptake to 10–12 % at 80 % RH. In NAL10L, a small mass drop at 60 % RH indicated the recrystallisation of amorphous leucine. This recrystallised leucine acted as a physical barrier to moisture penetration, as crystalline leucine is non-hygroscopic and has a low propensity for water uptake (Chang and Chan, 2022). Similar protective effects and leucine recrystallisation at 60 % RH have been observed in other spray dried powders, such as salbutamol sulfate (Li et al., 2017) and disodium cromoglycate (Li et al., 2016) with 5–20 % w/w leucine. In contrast, NAL20L only showed one recrystallisation event at 80 % RH because leucine was crystalline in the formulation, consistent with the faint peak observed at 6° in the XRD results in Fig. 4. On the other hand, NAL10HSA absorbed more moisture than SD NAL and both leucine-containing formulations at 80 % RH, owing to the high hygroscopicity of HSA. Interestingly, HSA delayed the recrystallisation of NAL20HSA until 90 % RH. This may be due to the high molecular weight of HSA, which limits molecular mobility and thus hinders crystallisation. Consequently, more water (acting as a plasticiser) was required to enable recrystallisation. Another possible explanation is the extent of particle surface coverage by the excipients. As depicted in the O-PTIR chemical overlaid maps in Fig. 3, HSA appeared to cover a larger portion of the particle surface than leucine at equivalent mass concentrations. Hence, HSA may absorb more moisture before enough accumulates to trigger recrystallisation of NAL in the formulation. Future studies are warranted to investigate the actual mechanism of how HSA delays moisture-induced recrystallisation. Nonetheless, the ability of HSA on delaying drug recrystallisation has also been reported previously (Tai et al., 2025).

Although all five spray dried powders were inhalable, SD NAL had the highest drug retention in the capsule and inhaler, as shown in Fig. 9. It also had the most drug deposition in the throat, potentially increasing the risk of local oropharyngeal adverse effects in patients. These findings indicated that the aerosol performance of SD NAL required improvement, warranting the need of excipients. Two commonly used excipients are leucine and HSA, which have previously been applied as dispersion enhancers (Chow et al., 2019; Li et al., 2017; Li et al., 2016; Li et al., 2025). Their effects were demonstrated not only by reducing capsule and inhaler retention and throat deposition but also by increasing drug deposition on the latter stages of the impactor. These improvements were observed with the addition of 10 % w/w excipient and became more pronounced at 20 % w/w. Compared to SD NAL, the other four formulations had more NAL deposited on Stages 1–3, resulting in larger MMADs. The only formulation with a comparable MMAD as SD NAL was NAL20L as it had more particles deposited at the latter stages of the NGI. The extensive deposition of NAL20L, ranging from Stage 1 to the micro-orifice collector, also explained its significantly broader GSD.

Among all five formulations, NAL20L achieved the highest EF (Fig. 10), FPDs (Fig. 11), and FPFs (Fig. 12) at both cutoff diameters (<5 and <3 μm), suggesting that it could potentially deliver the most NAL to the lungs and systemic circulation. This also implied that leucine was a more effective dispersion enhancer than HSA. In fact, the FPF <5 μm of NAL10L (39 %) was comparable to those of both NAL10HSA (33 %) and NAL20HSA (37 %), indicating that 10 % w/w leucine was almost as effective as 20 % w/w HSA. For FPF <3 μm, both HSA-containing formulations did not show any significant improvement compared to SD NAL, indicating that HSA had limited ability to enhance the fraction of fine particles <3 μm. This may be explained by the less corrugated particle surfaces of NAL10HSA and NAL20HSA. Reduced particle corrugation increases contact surface area and interparticle cohesion, which in turn worsens aerosol performance (Chew and Chan, 2001). Interestingly, the powder densities and Carr's index in Table 4 suggested that NAL10L was the least cohesive among all the spray dried powders (and therefore expected to disperse well), while the addition of excipients increased the powder cohesiveness (and was thus believed to have lower FPFs). However, the trends in bulk and tapped densities and Carr's index did not correspond to those of the FPFs. This discrepancy arises because Carr's index assesses the flowability of powders with discrete particles (Seville et al., 2007). In contrast, spray dried powders typically form aggregates with varying strengths, which can lead to misleading Carr's index value and inaccurate flowability classification. Therefore, bulk and tapped densities and Carr's index cannot reliably predict aerosol performance. This limitation was also reported in another study, which showed a lack of correlation between FPF and Carr's index in co-spray dried salbutamol sulfate and lactose formulations containing various amino acids (i.e. arginine, leucine, and phenylalanine) (Seville et al., 2007). Nonetheless, increasing the proportion of leucine or HSA from 10 % to 20 % w/w in the formulations enhances surface enrichment during spray drying (as confirmed by the O-PTIR chemical maps in Fig. 3), thus reducing particle cohesion more effectively and improving aerosol performance. Besides promoting powder dispersibility, the addition of leucine also contributed to the chemical and physical stability of the powders during storage (Chang et al., 2019). This was supported by the stability test results in Fig. 13, which showed no significant drug degradation or statistical differences in FPFs <5 and <3 μm after storage at 25 °C/30 % RH and 25 °C/60 % RH for one month. The good stability of NAL20L highlights the potential of dry powder formulations to address concerns related to NAL degradation in solution, such as in nasal formulations like Apain®. Further long-term stability studies are required to confirm the shelf-life of NAL20L under various storage conditions.

The feasibility of clinical use of the formulations can be estimated using *in vitro* FPD, although this may not represent the actual inhaled dose *in vivo* (Newman and Chan, 2020). While NAL has some potential local therapeutic effects in the lungs, its primary indication is for analgesia, which requires the drug particles to reach the small airways or alveoli for systemic absorption. Hence, the FPD <3 μm of NAL20L (5.1 mg per capsule) was used for dose estimation. The recommended dose of NAL injection for a 70 kg adult is 10 mg, which can be repeated every 3 to 6 h when required (Pfizer, 2025). A similar intranasal dose (10.5 mg) has also been used in human PK and efficacy studies (Tymko et al., 2024; Tymko et al., 2023). While this intranasal requires three puffs of spray (as per the PK study), patients would only need to inhale two capsules to NAL20L to receive an equivalent dose (10.2 mg). Inhaling two capsules every 3–6 h is practical, as similar dosing regimens are already used with commercial inhalers, such as Ventolin® metered dose inhaler (salbutamol sulfate; one to two puffs every 4 to 6 h when needed) (GlaxoSmithKline Pharmaceuticals, 2025) and Bricanyl® Turbuhaler® (terbutaline; one to three inhalations every 4 to 6 h when required) (NPS Medicinewise, 2025). Therefore, inhalable NAL powders may offer a feasible alternative to injection or intranasal administration, potentially improving pain management and patient adherence. Further studies are warranted to investigate the PK profiles of the inhalable spray dried NAL powders.

5. Conclusions

NAL powders, with and without leucine and HSA, were successfully produced via spray drying. The spray dried formulations exhibited good production yields and were inhalable. The addition of leucine and HSA further increased surface roughness, which enhanced powder aerosolisation. Compared to HSA, leucine was more effective at enhancing the aerosol performance. These formulations can be used as a platform to deliver NAL and other opioid analgesics by inhalation.

Declaration of Generative AI and AI-assisted technologies in the writing process

During the preparation of this work the author(s) used ChatGPT in

order to improve the readability and language of the manuscript. After using this tool/service, the author(s) reviewed and edited the content as needed and take(s) full responsibility for the content of the published article.

CRediT authorship contribution statement

Waiting Tai: Writing – original draft, Methodology, Investigation, Data curation, Conceptualization. **Hong-Jaan Wang:** Writing – review & editing, Conceptualization. **Dipesh Khanal:** Writing – review & editing, Investigation. **Pancy Tsz Hei Kwong:** Writing – review & editing, Investigation. **Patricia Tang:** Writing – review & editing, Conceptualization. **Chih-Chin Shih:** Writing – review & editing, Supervision, Methodology, Investigation, Conceptualization. **Hak-Kim Chan:** Writing – review & editing, Supervision, Methodology, Conceptualization.

Declaration of competing interest

The authors declare that they have no known competing financial interests or personal relationships that could have appeared to influence the work reported in this paper.

Acknowledgements

The authors would like to thank Dr. Philip Chi Lip Kwok for his valuable comments and insights to this study.

Data availability

Data will be made available on request.

References

Alhajj, N., O'Reilly, N.J., Cathcart, H., 2021. Leucine as an excipient in spray dried powder for inhalation. Drug Discov. Today 26 (10), 2384–2396. https://doi.org/10.1016/j.drudis.2021.04.009.

Bhujbal, S.V., Mitra, B., Jain, U., Gong, Y., Agrawal, A., Shyam Karki, S., Taylor, L.S., Kumar, S., Zhou, Q.T., 2021. Pharmaceutical amorphous solid dispersion: a review of manufacturing strategies. Acta Pharm. Sin. B 11 (8), 2505–2536. https://doi.org/10.1016/j.apsb.2021.05.014.

Bosquillon, C., Lombry, C., Preat, V., Vanbever, R., 2001. Influence of formulation excipients and physical characteristics of inhalation dry powders on their aerosolization performance. J. Control. Release 70 (3), 329–339. https://doi.org/10.1016/s0168-3659(00)00362-x.

Chang, R.Y.K., Chan, H.K., 2022. Advancements in particle engineering for inhalation delivery of small molecules and biotherapeutics. Pharm. Res. 39 (12), 3047–3061. https://doi.org/10.1007/s11095-022-03363-2.

Chang, R.Y.K., Li, M., Chow, M.Y.T., Ke, W.R., Tai, W., Chan, H.K., 2022. A dual action of D-amino acids on anti-biofilm activity and moisture-protection of inhalable ciprofloxacin powders. Eur. J. Pharm. Biopharm. 173, 132–140. https://doi.org/10.1016/j.ejpb.2022.03.003.

Chang, R.Y.K., Wallin, M., Kutter, E., Morales, S., Britton, W., Li, J., Chan, H.K., 2019. Storage stability of inhalable phage powders containing lactose at ambient conditions. Int. J. Pharm. 560, 11–18. https://doi.org/10.1016/j.ijpharm.2019.01.050.

Chen, Y.L., Lai, Y.H., Huang, E.Y., Wang, H.J., Hung, H.Y., 2024. Nalbuphine-6-glucuronide is a potent analgesic with superior safety profiles by altering binding affinity and selectivity for mu-/kappa-opioid receptors. Life Sci. 340, 122441. https://doi.org/10.1016/j.lfs.2024.122441.

Chew, N.Y., Chan, H.K., 2001. Use of solid corrugated particles to enhance powder aerosol performance. Pharm. Res. 18 (11), 1570–1577. https://doi.org/10.1023/a:1013082531394.

Chow, M.Y.T., Qiu, Y., Liao, Q., Kwok, P.C.L., Chow, S.F., Chan, H.K., Lam, J.K.W., 2019. High siRNA loading powder for inhalation prepared by co-spray drying with human serum albumin. Int. J. Pharm. 572, 118818. https://doi.org/10.1016/j.ijpharm.2019.118818.

Dershwitz, M., Walsh, J.L., Morishige, R.J., Connors, P.M., Rubsamen, R.M., Shafer, S.L., Rosow, C.E., 2000. Pharmacokinetics and pharmacodynamics of inhaled versus intravenous morphine in healthy volunteers. Anesthesiology 93 (3), 619–628. https://doi.org/10.1097/00000542-200009000-00009.

GlaxoSmithKline Pharmaceuticals, 2025, Ventolin HFA (albuterol sulfate inhalation aerosol), for oral inhalation use - Prescribing information. https://gskpro.com/content/dam/global/hcpportal/en_US/Prescribing_Information/Ventolin_HFA/pdf/VENTOLIN-HFA-PI-PIL-IFU.PDF (accessed 7th May 2025).

Hanko, J., Vlahova, P., 2011. Crystalline and amorphous forms of nalbuphine hydrochloride, US8536191B2.

Ke, W.R., Chang, R.Y.K., Chan, H.K., 2022. Engineering the right formulation for enhanced drug delivery. Adv. Drug Deliv. Rev. 191, 114561. https://doi.org/10.1016/j.addr.2022.114561.

Khanna, K., Sharma, N., Karwasra, R., Kumar, A., Nishad, D.K., Janakiraman, A.K., Ram Mani, R., Rajagopal, M., Tayyab, S., Goel, B., 2025. Exploring nalbuphine loaded chitosan nanoparticles for effective pain management through intranasal administration: a comparative study. J. Drug Target. 33 (1), 99–110. https://doi.org/10.1080/1061186X.2024.2397800.

Kuznetsov, I.E., Tymko, V.G., 2023. Nalbuphine nasal spray: proven medication and new capabilities. J. Basic Clin. Pharma. 14 (4), 290–293.

Kuznetsov, I.E., Tymko, V.G., 2024. Nalbuphine nasal spray: analgesic efficacy and safety. J. Pharm. Pharm. Res. 8 (2), 011. 10.21767/ipipr.8.02.011.

Kuzumaki, N., Suzuki, A., Narita, M., Hosoya, T., Nagasawa, A., Imai, S., Yamamizu, K., Morita, H., Nagase, H., Okada, Y., Okano, H.J., Yamashita, J.K., Okano, H., Suzuki, T., Narita, M., 2012. Effect of kappa-opioid receptor agonist on the growth of non-small cell lung cancer (NSCLC) cells. Br. J. Cancer 106 (6), 1148–1152. https://doi.org/10.1038/bjc.2011.574.

Li, L., Leung, S.S.Y., Gengenbach, T., Yu, J., Gao, G.F., Tang, P., Zhou, Q.T., Chan, H.K., 2017. Investigation of L-leucine in reducing the moisture-induced deterioration of spray-dried salbutamol sulfate power for inhalation. Int. J. Pharm. 530 (1–2), 30–39. https://doi.org/10.1016/j.ijpharm.2017.07.033.

Li, L., Sun, S., Parumasivam, T., Denman, J.A., Gengenbach, T., Tang, P., Mao, S., Chan, H.K., 2016. L-Leucine as an excipient against moisture on in vitro aerosolization performances of highly hygroscopic spray-dried powders. Eur. J. Pharm. Biopharm. 102, 132–141. https://doi.org/10.1016/j.ejpb.2016.02.010.

Li, M., Cao, Y., Chan, H.K., 2025. Optimizing performance of inhalable bacteriophage powders using human serum albumin (HSA). Int. J. Pharm. 125709. https://doi.org/10.1016/j.ijpharm.2025.125709.

Liang, R.J., Shih, Y.N., Chen, Y.L., Liu, W.Y., Yang, W.L., Lee, S.Y., Wang, H.J., 2020. A dual system platform for drug metabolism: Nalbuphine as a model compound. Eur. J. Pharm. Sci. 141, 105093. https://doi.org/10.1016/j.ejps.2019.105093.

Lu, W., Rades, T., Rantanen, J., Yang, M., 2019. Inhalable co-amorphous budesonide-arginine dry powders prepared by spray drying. Int. J. Pharm. 565, 1–8. https://doi.org/10.1016/j.ijpharm.2019.04.036.

Maa, Y.F., Costantino, H.R., Nguyen, P.A., Hsu, C.C., 1997. The effect of operating and formulation variables on the morphology of spray-dried protein particles. Pharm. Dev. Technol. 2 (3), 213–223. https://doi.org/10.3109/10837459709031441.

Macleod, D.B., Habib, A.S., Ikeda, K., Spyker, D.A., Cassella, J.V., Ho, K.Y., Gan, T.J., 2012. Inhaled fentanyl aerosol in healthy volunteers: pharmacokinetics and pharmacodynamics. Anesth. Analg. 115 (5), 1071–1077. https://doi.org/10.1213/ANE.0b013e3182691898.

Maher, T.M., Avram, C., Bortey, E., Hart, S.P., Hirani, N., Molyneux, P.L., Porter, J.C., Smith, J.A., Sciascia, T., 2023. Nalbuphine tablets for cough in patients with idiopathic pulmonary fibrosis. NEJM Evid. 2 (8), EVIDoa2300083. https://doi.org/10.1056/EVIDoa2300083.

Marante, T., Viegas, C., Duarte, I., Macedo, A.S., Fonte, P., 2020. An overview on spray-drying of protein-loaded polymeric nanoparticles for dry powder inhalation. Pharmaceutics 12 (11), 1032. https://doi.org/10.3390/pharmaceutics12111032.

Mestek, O., 2025, Infrared Spectroscopy. https://uanlch.vscht.cz/files/uzel/0052236/0003~~8wxSiDcyMDAHAA.pdf?redirected (accessed 3rd July 2025).

Murphy, G., Brayden, D.J., Cheung, D.L., Liew, A., Fitzgerald, M., Pandit, A., 2025. Albumin-based delivery systems: recent advances, challenges, and opportunities. J. Control. Release 380, 375–395. https://doi.org/10.1016/j.jconrel.2025.01.035.

Narver, H.L., 2015. Nalbuphine, a non-controlled opioid analgesic, and its potential use in research mice. Lab. Anim. (N.Y.) 44 (3), 106–110. https://doi.org/10.1038/laban.701.

Newman, A.W., Reutzel-Edens, S.M., Zografi, G., 2008. Characterization of the "hygroscopic" properties of active pharmaceutical ingredients. J. Pharm. Sci. 97 (3), 1047–1059. https://doi.org/10.1002/jps.21033.

Newman, S.P., Chan, H.K., 2020. In vitro-in vivo correlations (IVIVCs) of deposition for drugs given by oral inhalation. Adv. Drug Deliv. Rev. 167, 135–147. https://doi.org/10.1016/j.addr.2020.06.023.

Medicinewise, 2025, Bricanyl® Turbuhaler® - Consumer medicine information. https://www.nps.org.au/assets/medicines/5e3ee333-7520-47ca-9829-a53300ff7a05.pdf (accessed 7th May 2025).

Ordoubadi, M., Shepard, K.B., Wang, H., Wang, Z., Pluntze, A.M., Churchman, J.P., Vehring, R., 2023. On the physical stability of leucine-containing spray-dried powders for respiratory drug delivery. Pharmaceutics 15 (2), 435. https://doi.org/10.3390/pharmaceutics15020435.

Pfizer, 2025, Nalbuphine hydrochloride injection - Prescribing information. https://labeling.pfizer.com/ShowLabeling.aspx?id=4505 (accessed 7th May 2025).

Pietsch, U., Berger, Y., Schurter, D., Theiler, L., Wenzel, V., Meuli, L., Grünenfelder, A., Albrecht, R., 2021. Nasal nalbuphine analgesia in prehospital trauma managed by first-responder personnel on ski slopes in Switzerland: an observational cohort study. SJTREM 29 (36). https://doi.org/10.1186/s13049-021-00852-y.

Pokorný, V., Červinka, C., Štejfa, V., Havlín, J., Růžička, K., Fulem, M., 2020. Heat capacities of L-alanine, L-valine, L-isoleucine, and L-leucine: experimental and computational study. J. Chem. Eng. Data 65 (4), 1833–1849. https://doi.org/10.1021/acs.jced.9b01086.

Schneider, C.A., Rasband, W.S., Eliceiri, K.W., 2012. NIH image to ImageJ: 25 years of image analysis. Nat. Methods 9 (7), 671–675. https://doi.org/10.1038/nmeth.2089.

Seville, P.C., Learoyd, T.P., Li, H.-Y., Williamson, I.J., Birchall, J.C., 2007. Amino acid-modified spray-dried powders with enhanced aerosolisation properties for

pulmonary drug delivery. Powder Technol. 178 (1), 40–50. https://doi.org/10.1016/j.powtec.2007.03.046.

Sun, X., Ma, S., Zang, Y.M., Lu, S.Y., Guo, H.T., Bi, H., Wang, Y.M., Ma, H., Ma, X.L., Pei, J.M., 2006. Vasorelaxing effect of U50,488H in pulmonary artery and underlying mechanism in rats. Life Sci. 78 (21), 2516–2522. https://doi.org/10.1016/j.lfs.2005.10.042.

Tai, W., Khanal, D., Arnold, J.C., Chan, H.K., Kwok, P.C.L., 2025. Solubilising and aerosolising cannabidiol using methyl beta-cyclodextrin and human serum albumin. AAPS PharmSciTech 26 (5), 120. https://doi.org/10.1208/s12249-025-03121-8.

Tai, W., Kwok, P.C.L., 2022. Recent advances in drug delivery to the central nervous system by inhalation. Expert. Opin. Drug Deliv. 19 (5), 539–558. https://doi.org/10.1080/17425247.2022.2074975.

Thompson, J.P., Thompson, D.F., 2016. Nebulized fentanyl in acute pain: a systematic review. Ann. Pharmacother. 50 (10), 882–891. https://doi.org/10.1177/1060028016659077.

Todisco, T., Dottorini, M., Palumbo, R., Calvitti, M., Vernelli, C., Rossi, F., Iannacci, L., Grandolini, S., Cosmi, E.V., 1990. Fate of human albumin microsphere and spherocyte radioaerosols in the human tracheobronchial tree. Lung 168 (Suppl), 665–671. https://doi.org/10.1007/BF02718192.

Tymko, V.G., Tsapko, G.V., Filipenko, V.A., Khvysiuk, O.M., Kovalova, K.V., Kuznetsov, I.E., 2024. A randomized, double-blind study to compare the efficacy and safety of nalbuphine nasal spray and injectable solution in patients after orthopaedic interventions and traumatological procedures. Br. J. Clin. Pharmacol. 90 (7), 1728–1740. https://doi.org/10.1111/bcp.16077.

Tymko, V.G., Tsapko, G.V., Kovalova, K.V., Mashchenko, S.V., Oliinykov, D.S., Kuznetsov, I.E., 2023. Comparative pharmacokinetics of nalbuphine nasal spray and solution for injection in healthy volunteers. Br. J. Clin. Pharmacol. 89 (11), 3311–3323. https://doi.org/10.1111/bcp.15828.

Wang, H.J., Hsiong, C.H., Ho, S.T., Lin, M.J., Shih, T.Y., Huang, P.W., Hu, O.Y.P., 2014. Commonly used excipients modulate UDP-Glucuronosyltransferase 2B7 activity to improve nalbuphine oral bioavailability in humans. Pharm. Res. 31 (7), 1676–1688. https://doi.org/10.1007/s11095-013-1272-4.

Wang, Y., Han, H.Y., Jia, Y.P., Zhao, L.Y., Li, Y., Zuo, B.J., Zhang, J., 2022. Protective effect of nalbuphine combined with dexmedetomidine on the lungs of children with atelectasis and foreign body in the bronchus during the perioperative period. Front. Physiol. 13, 799183. https://doi.org/10.3389/fphys.2022.799183.

Ward, M.E., Woodhouse, A., Mather, L.E., Farr, S.J., Okikawa, J.K., Lloyd, P., Schuster, J. A., Rubsamen, R.M., 1997. Morphine pharmacokinetics after pulmonary administration from a novel aerosol delivery system. Clin. Pharmacol. Ther. 62 (6), 596–609. https://doi.org/10.1016/S0009-9236(97)90079-5.

Yang, M.Y., Verschuer, J., Shi, Y., Song, Y., Katsifis, A., Eberl, S., Wong, K., Brannan, J.D., Cai, W., Finlay, W.H., Chan, H.K., 2016. The effect of device resistance and inhalation flow rate on the lung deposition of orally inhaled mannitol dry powder. Int. J. Pharm. 513 (1–2), 294–301. https://doi.org/10.1016/j.ijpharm.2016.09.047.

Zeng, S., Zhong, Y., Xiao, J., Ji, J., Xi, J., Wei, X., Liu, R., 2020. Kappa opioid receptor on pulmonary macrophages and immune function. Transl. Perioper. Pain Med. 7 (3), 225–233. https://doi.org/10.31480/2330-4871/117.

Zhang, Y., Jiang, Q., Li, T., 2017. Nalbuphine analgesic and anti-inflammatory effects on patients undergoing thoracoscopic lobectomy during the perioperative period. Exp. Ther. Med. 14 (4), 3117–3121. https://doi.org/10.3892/etm.2017.4920.